



OPEN

A novel strategy for stabilization of sub-nanometric Pd colloids on kryptofix functionalized MCM-41: nanoengineered material for Stille coupling transformation

Hassan Alamgholiloo¹, Nader Noroozi Pesyan¹ & Sadegh Rostamnia²

The stabilization of sub-nanometric metal particles (<1 nm) with suitable distribution remained challenging in the catalytic arena. Herein, an intelligent strategy was described to anchoring and stabilizing sub-nanometric Pd colloids with an average size of 0.88 nm onto Kryptofix 23 functionalized MCM-41. Then, the catalytic activity of Pd@Kryf/MCM-41 was developed in Stille coupling reaction with a turnover frequency (TOF) value of 247 h⁻¹. The findings demonstrate that porous MCM-41 structure and high-affinity Kryptofix 23 ligand toward adsorption of Pd colloids has a vital role in stabilizing the sub-nanometric particles and subsequent catalytic activity. Overall, these results suggest that Pd@Kryf/MCM-41 is a greener, more suitable option for large-scale applications and provides new insights into the stabilization of sub-nanometric metal particles.

Within the field of silica-based materials, MCM-41 as a nanoreactor has possessed much attention in the catalytic process arena due to unique properties such as high surface areas, chemical stability, and structural rigidity¹⁻³. Furthermore, these porous materials can be an excellent candidate for the stabilization of metal nanoparticles (NPs) as a heterogeneous catalyst in modern synthesis⁴⁻⁶. Recently, efforts have been made for the fabrication of metal NPs in MCM-41, and these nanostructures demonstrated potential utility in catalytic processes⁷⁻⁹. Therefore, a simple, inexpensive, and efficient synthetic method that facilitates the immobilization of metal NPs in MCM-type solid materials is required.

The cryptand compounds known also with the commercial name Kryptofix are frequently used in host-guest chemistry¹⁰⁻¹⁴. 1,4,7,13,16-Pentaoxa-10,19-diazacycloheneicosane (Kryptofix 23) as a specific class of aza-crown ether have been known for their high affinity to bind spherical cations. They are macro-bicyclic ligands that contain an internal cavity of about spherical shape and provide very stable and selective complexes with a variety of metal cations¹⁵. These ligands are exceptionally versatile in selectively binding a range of metal ions and led to the development of host-guest chemistry.

Recently, the application of colloidal metal nanoparticles has become a promising approach for catalytic applications. Various techniques such as capping agents, surfactants, and organic ligands have been applied for the preparation and stability of colloidal nanoparticles to overcome aggregate problems¹⁶⁻¹⁹. Among the methods mentioned above, crown ether macrocyclic compounds have an excellent capacity to adsorb metal ions²⁰⁻²³. Therefore, it is an excellent candidate for the anchoring and stabilization of colloidal metal nanoparticles. Recently, Verport and co-workers developed the loading of metallic Pd nanocrystals on azobenzene-based colloidal porous organic polymer for photocatalytic Suzuki coupling reaction²⁴. In parallel, Shi and co-workers explored the synthesis of Pd colloids grafted mesoporous silica materials SBA-15 in Mizoroki-Heck reactions²⁵. Moreover, the authors' previous study^{17,19,26-28} and other studies²⁹⁻³⁷ have proven that colloidal Pd, Pd NPs, and Pd complex can greatly boost C-C bond formations.

Considering the unique metal colloid structure, we have envisioned an intelligent method for anchoring and stabilizing sub-nanometric Pd onto Kryptofix 23 functionalized MCM-41. We also demonstrated the catalytic activity of this nanostructure in the carbon-carbon coupling reaction. To the best of our knowledge, this is the

¹Department of Organic Chemistry, Faculty of Chemistry, Urmia University, 57159 Urmia, Iran. ²Organic and Nano Group (ONG), Department of Chemistry, Iran University of Science and Technology (IUST), PO Box, 16846-13114 Tehran, Iran. ✉email: nnp403@gmail.com; rostamnia@iust.ac.ir

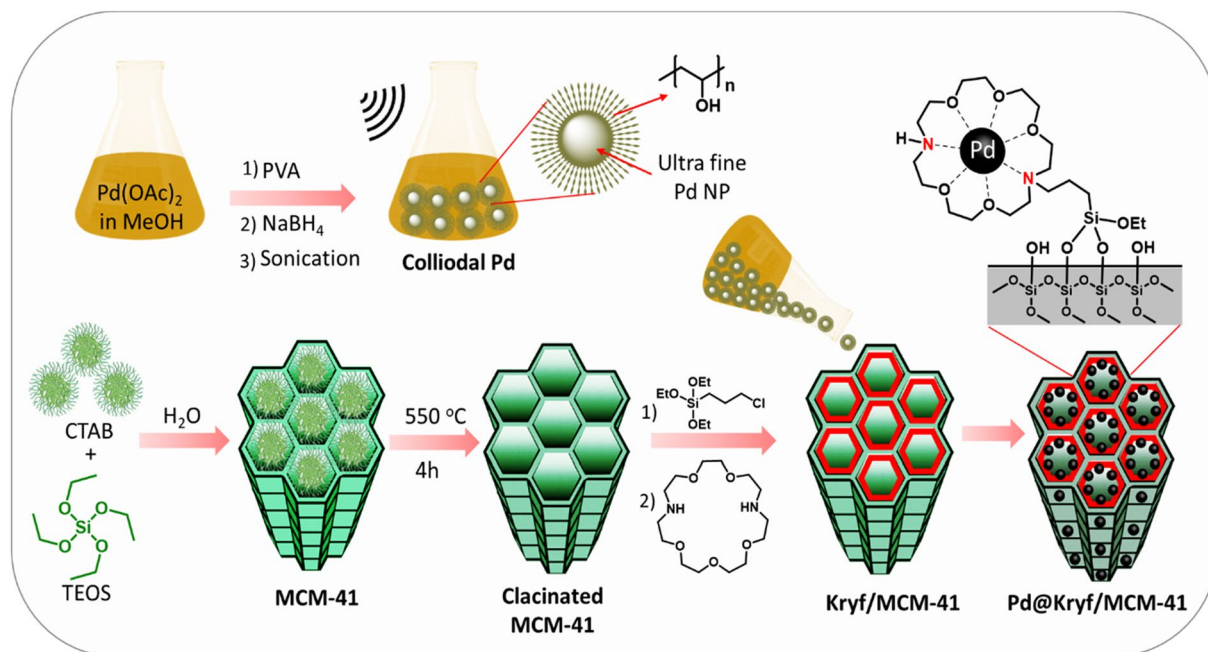


Figure 1. Synthetic pathway of Pd@Kryf/MCM-41.

first example of the stabilization of sub-nanometric Pd colloids with crown ether macrocyclic compounds that exhibit enhanced catalytic activity in the Stille coupling reaction. The current study widens the applications of sub-nanometric metal particles for catalytic process.

Experimental

Synthesis of Kryf/MCM-41 mesoporous. The nanoporous MCM-41 was prepared with a sol–gel method according to our previous report^{38,39} (Detailed in Support Information). Initially, 2.0 g calcinated MCM-41 was dissolved in 30 mL toluene solutions under the reflux condition at 12 h. Then, 10 mmol (2.4 mL) (3-chloropropyl) triethoxysilane was added to the mixture reaction under stir for 24 h. The prepared powder from the reaction was washed with ethanol several times, which obtain MCM-41-Cl with loading 56.5% linker. After that, 0.5 mL of Kryptofix 23 and 1.0 ml Et₃N in 20 ml EtOH was added to 1.5 g MCM-41-Cl under reflux condition. After stirring for 24 h, the mixture was washed several times with EtOH. Finally, it was dried in a vacuum at 80 °C for 12 h, and a 61% yield of Kryf/MCM-41 was synthesized.

Preparation of Pd@Kryf/MCM-41. The colloidal Pd NPs was synthesized by using the impregnation reduction method according to our previous report with some modification¹⁹. First, 0.02 g Pd (OAc)₂ (Pd: 47.5%) and 0.2 g polyvinyl alcohol PVA was dispersed in 15 mL MeOH under sonication for 30 min. Subsequently, 5.0 mL 0.1 M of NaBH₄ was poured into the mixture mentioned above to fabricate a colloidal Pd solution. After stirring for 60 min under ambient conditions, 1.0 g Kryf/MCM-41 was added to the mixture. After stirring for 4 h at ambient conditions, the final solid result was collected by filtration and washed with EtOH several times then dried at room temperature. Wt% of Pd in the Kryf/MCM-41 mesoporous was calculated via inductively coupled plasma optical emission spectrometry (ICP-OES), and the resultant yield indicated 0.72%.

General procedure for Stille coupling reactions. In the model reaction, the mixture of aryl halides (3 mmol), triphenyltin chloride (1 mmol), Na₂CO₃ (3 mmol), polyethylene glycol-400 (PEG-400, 2 mL) was added to 0.36 mol% Pd@Kryf/MCM-41 catalyst. The reaction vessel was capped and allowed to stir at room temperature for 3 h. After the reaction is complete, the organic phase was extracted with ethyl acetate/petroleum ether (1:2) and dried over sodium sulfate (Na₂SO₄) to obtain the corresponding biphenyl. Finally, all biaryls were identified by ¹H and ¹³C-NMR spectroscopy and comparison with the literature^{28,40}.

Results and discussion

In addition to the scientific findings in introducing engineered nanomaterials^{41–46}, herein, Pd@Kryf/MCM-41 mesoporous silica was presented for Stille coupling reaction (Fig. 1). Our initial efforts were geared towards preparing MCM-41 mesoporous silica material via the sol–gel method, which was followed by grafting Kryptofix 23 into pores of MCM-41. Finally, Kryf/MCM-41 was then utilized as excellent support for immobilizing colloidal Pd NPs in the sub-nanometer scale.

Structural and morphology characterization. First, the crystalline structure of Kryf/MCM-41 and Pd@Kryf/MCM-41 was analyzed using the powder XRD pattern. In a small-angle XRD (SA-XRD) pattern of

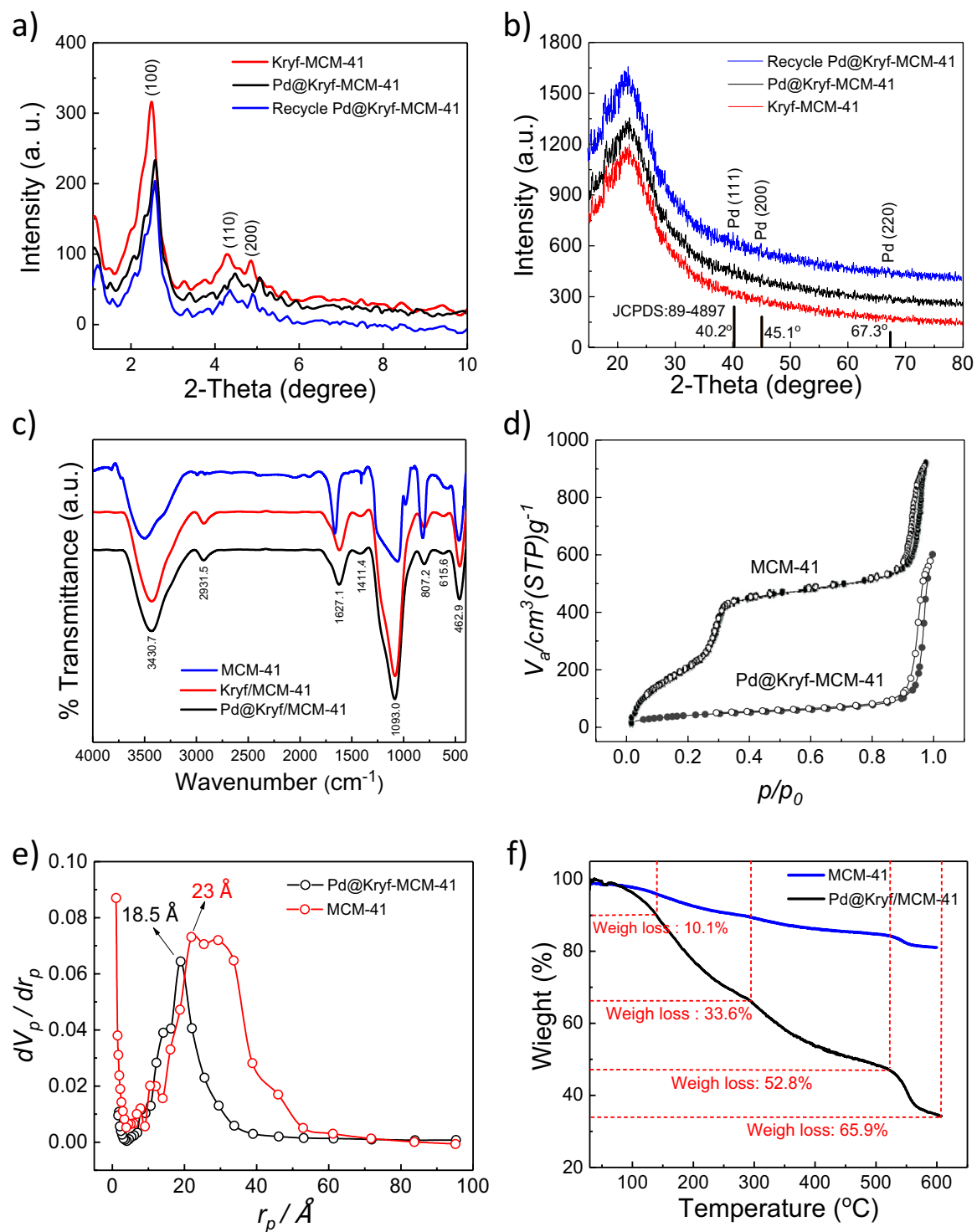


Figure 2. SA-XRD and WA-XRD patterns for Kryf/MCM-41, Pd@Kryf/MCM-41 and recycled Pd@Kryf/MCM-41 (a, b); FT-IR of MCM-41, Kryf/MCM-41, and Pd@Kryf/MCM-41 (c); N₂ adsorption-desorption profile (d); BJH plot (e); and TGA curves of MCM-41 and Pd@Kryf/MCM-41 (f).

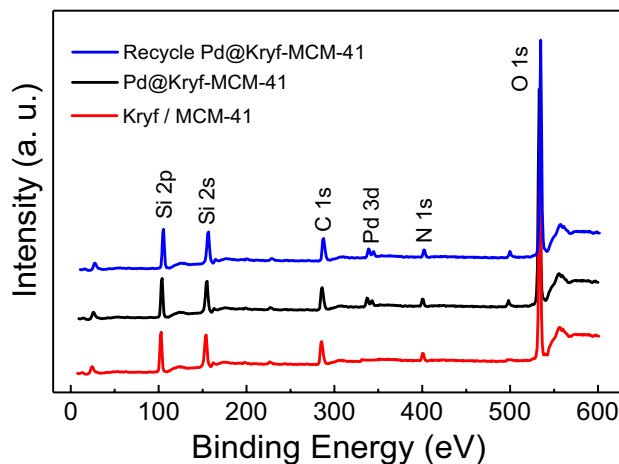


Figure 3. XPS spectra of Kryf/MCM-41, Pd@Kryf/MCM-41, and recycled Pd@Kryf/MCM-41.

Kryf-MCM-41, the characteristic diffraction peaks at $2.3\text{--}4.7^\circ$ for the planes (100), (110), and (200) can be indexed 2D-hexagonal $p6mm$ pore MCM-41 structure⁴⁷, while these peaks in Pd@Kryf/MCM-41 was reduced and slightly shifted to relatively high 2θ region^{3,48} (Fig. 2a). In a wide-angle XRD (WA-XRD) pattern, a broad peak that appeared under the condition $2\theta = 23.9^\circ$ is consistent with the amorphous nature of the pore wall of MCM-41 structure^{49,50}. Also, three peaks that appeared under the condition $2\theta = 40.2^\circ$, 45.1° , and 67.3° are consistent with those of the crystal planes of Pd NPs (JCPDS 89-4897) (Fig. 2b). Furthermore, according to the Scherrer equation, the average crystalline size of Pd was found to be ~ 0.88 nm (Table S1, ESI), which demonstrated that sub-nanometric particles. Moreover, the formation of sub-nanometric Pd was confirmed further by and high-resolution TEM (HR-TEM) and STEM mapping microscopy.

Subsequently, chemical groups of these meso-structures were studied by Fourier transform infrared (FT-IR) spectra (Fig. 2c). The peaks observed at 3430 cm^{-1} and 1627 cm^{-1} can be attributed to hydroxyl groups and adsorbed water⁵¹, respectively. The absorption band in 2931 cm^{-1} can be ascribed to the CH_2 -stretching vibration peak of Kryptofix 23 and the *n*-propyl aliphatic chain. Also, the peaks observed at 1411 cm^{-1} after the functionalization of MCM-41 with Kryptofix 23 confirms the covalent bonding crown ether ligand to the surface mesoporous silica.

The porosity properties of Pd@Kryf/MCM-41 were measured using the isotherm and Brunauer–Emmett–Teller (BET) plot. MCM-41 had a surface area of $990\text{ cm}^2/\text{g}^{-1}$, a pore volume of $1.306\text{ cm}^3/\text{g}$, and pore size of 4.6 nm (Table S2, ESI). Meanwhile, Pd@Kryf/MCM-41 surface area, pore volume, and pore size were $601\text{ cm}^2/\text{g}^{-1}$, $0.886\text{ cm}^3/\text{g}$, and 3.7 nm , which reflects the presence of the meso-size pores (Fig. 2d,e). Moreover, decrease surface area Pd@Kryf/MCM-41 was attributed to the loading of crown ether compound and Pd NPs.

TGA curves of MCM-41 and Pd@Kryf/MCM-41 demonstrate the weight loss of the organic material and thermal stability of Kryptofix 23 ligand in MCM-41. Figure 2f illustrates four weight loss steps in the TGA curve of Pd@Kryf/MCM-41 catalysts. The first weight loss (10.1%) between 30 and 140°C is occurred due to the removal of adsorbed water moisture at the surface. The next weight loss (33.6%) from 140 to 295°C is due to the decomposition of organic material and burning of ligand, which can be found that Kryptofix 23 material is relatively stable below 295°C . After 295°C , the phase remains completely changed, which was stable up to over 510°C .

The interaction between Pd NPs with Kryf/MCM-41 was further investigated by XPS spectrum (Fig. 3). As for Kryf/MCM-41 meso-structure, the C 1s and N 1s XPS spectra in 285.5 and 399.1 eV , indicating to the thoroughly immobilized Kryptofix 23 ligand in MCM-41 surface. Meanwhile, the appearance of the Pd 3d XPS spectrum in $336\text{--}342\text{ eV}$, confirming the successful coordination of colloidal Pd NPs in Kryf/MCM-41.

Field emission scanning electron microscopy (FESEM) image of the prepared Kryf/MCM-41 and Pd@Kryf/MCM-41 shows round-shaped particles with a mean diameter of $\sim 22\text{ nm}$ (Fig. 4a,b). After the deposition of colloidal Pd NPs on the surface of Kryf/MCM-41, the structures of the round-shaped particles were preserved, indicating that NPs were anchored in an orderly manner (Fig. 4b). The surface of MCM-41 with Kryptofix 23 ligand helped stabilize Pd NPs and inhibition the agglomeration. Besides, the round-shaped morphology of Kryf/MCM-41 and Pd@Kryf/MCM-41 was further confirmed with colored FESEM and Atomic Force Microscope (AFM) (Fig. 4c–f).

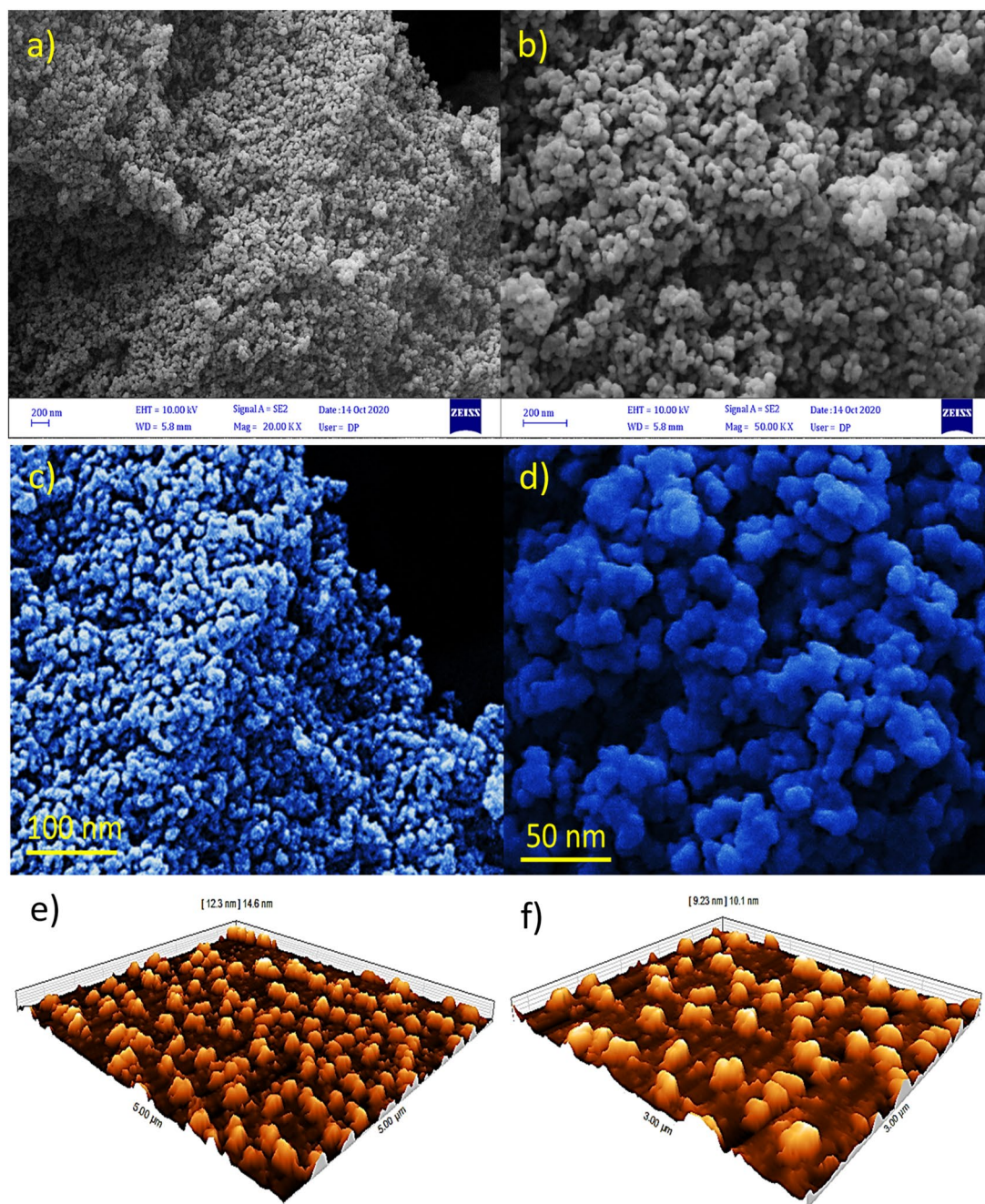


Figure 4. FESEM micrograph (a, b); colored FESEM (c, d); AFM images of Kryf/MCM-41 and Pd@Kryf/MCM-41 (e, f).

The Pd particles are not observable using FESEM measurements, so transmission electron microscopy (TEM) was employed to elucidate the morphology further and loading NPs on the mesoporous silica surface. As depicted in the TEM images, Kryf/MCM-41 and Pd@Kryf/MCM-41 possessed distinct regular channeling pores of 2D-hexagonal pore structure (Fig. 5a–c), which is confirmed with XRD pattern. The high magnifier image (~15 nm, Fig. 5d) indicates the formation of NPs in Kryf/MCM-41 surface without any agglomeration. When only MCM-41 was used for the deposition instead of Kryptofix 23 functionalized, an agglomeration of Pd

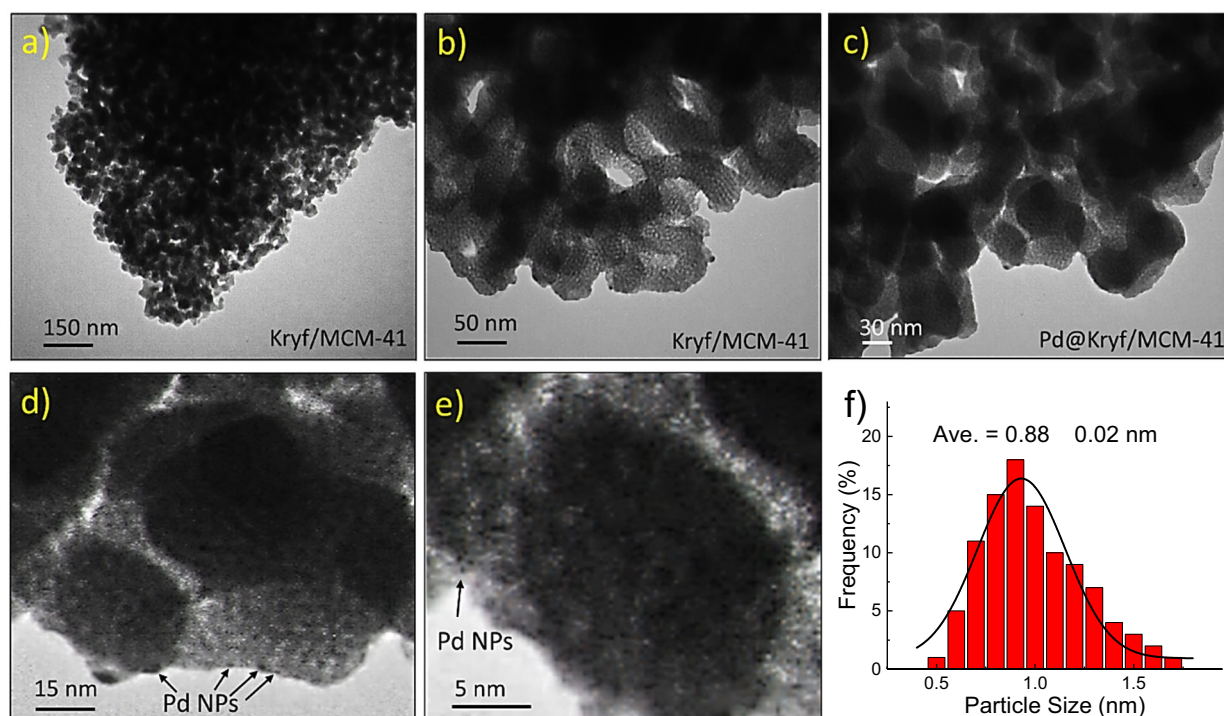


Figure 5. TEM images of Kryf/MCM-41 (a, b); Pd@Kryf/MCM-41 (c, d); HR-TEM of Pd@Kryf/MCM-41 (e); and corresponding size distributions of Pd NPs (f).

NPs with relatively bigger particle sizes were observed on the surface of MCM-41 (Fig. S1, ESI). A close inspection of HR-TEM image confirms the formation of NPs (Fig. 5e). Moreover, the statistical count of the particle size of Pd (> 100 counts and Gauss fit) in Kryf/MCM-41 surface was determined to be 0.88 ± 0.02 nm (Fig. 5f).

In addition to FESEM and TEM images, the STEM spectrum exhibit more detail about the deposition of Pd NPs onto the mesoporous material (Fig. 6a–f). The dark-field STEM images of Pd@Kryf/MCM-41 can be affirmed that the Pd particles are homogeneously deposited onto the Kryf/MCM-41 mesoporous. Meanwhile, STEM mapping images and energy dispersive X-ray (EDX) analysis, confirm the presence of all constituent elements (i.e., Si, O, C, N, and Pd) in the mesoporous structure (Fig. 6g).

Catalytic activity of Pd@Kryf/MCM-41. The importance of the coupling reactions in pharmaceutical synthesis has led to broad interdisciplinary attention research^{52,53}. On the other hand, the Stille coupling reaction due to harsh reaction conditions such as high temperature, inert atmosphere, and use of toxic solvents has caused a great challenge in the carbon–carbon coupling reactions. Therefore, after full identification of Pd@Kryf/MCM-41, employing this nanostructure for the green synthesis of biaryls was paid attention (Fig. 7).

The experiments indicated that in the absence of Pd@Kryf/MCM-41 not afford the desired product (Table 1, entry 1). When the amount of Pd@Kryf/MCM-41 increased to 0.01 g (0.36 mol% Pd) in the presence of 1 equivalent Na_2CO_3 , the yield production was also increased up to 66% (Table 1, entry 2). Therefore, by increasing the amount of Na_2CO_3 to 3 equivalent, the yield was improved to 96% within 3 h, indicating a better conversion in comparison to the best catalyst systems (Table 3). However, different base was applied for the optimization such as $\text{N}(\text{Et})_3$, NaHCO_3 , CaCO_3 , NaOH , and Na_2CO_3 . Among all the screened bases, it was observed that Na_2CO_3 gave a higher conversion of biaryls. After screening different solvents in optimized conditions, PEG-400 as a green solvent turned out to give the best conversion. This solvent proved to have many applications in reaction such as oxidation⁵⁴, reduction^{55,56}, addition⁵⁷, substitution⁵⁸, coupling^{17,59}, and etc. Also, solvents nonpolar like Toluene, *n*-Hexane, and dioxane were investigated and revealed slight conversion (Table 1, entries 8–10). Besides, DMSO, DMF, EtOH, and H_2O gave moderate conversion of biaryls (Table 1, entries 11–14). On the other hand, Pd^{2+} @MCM-41 and Pd^{2+} @Kryf/MCM-41 result in a moderate conversion (Table 1, entries 15 and 16). When colloidal Pd NPs immobilize in Kryf/MCM-41 with particle size 0.88 nm demonstrate that they deliver the product with more than 96% yield within 3 h. Ultimately, by increasing the temperature reaction from ambient condition to 120 °C, a slight increase in the yield of the reaction was observed (Table 1, entry 17), indicating the mildness and convenience of operation.

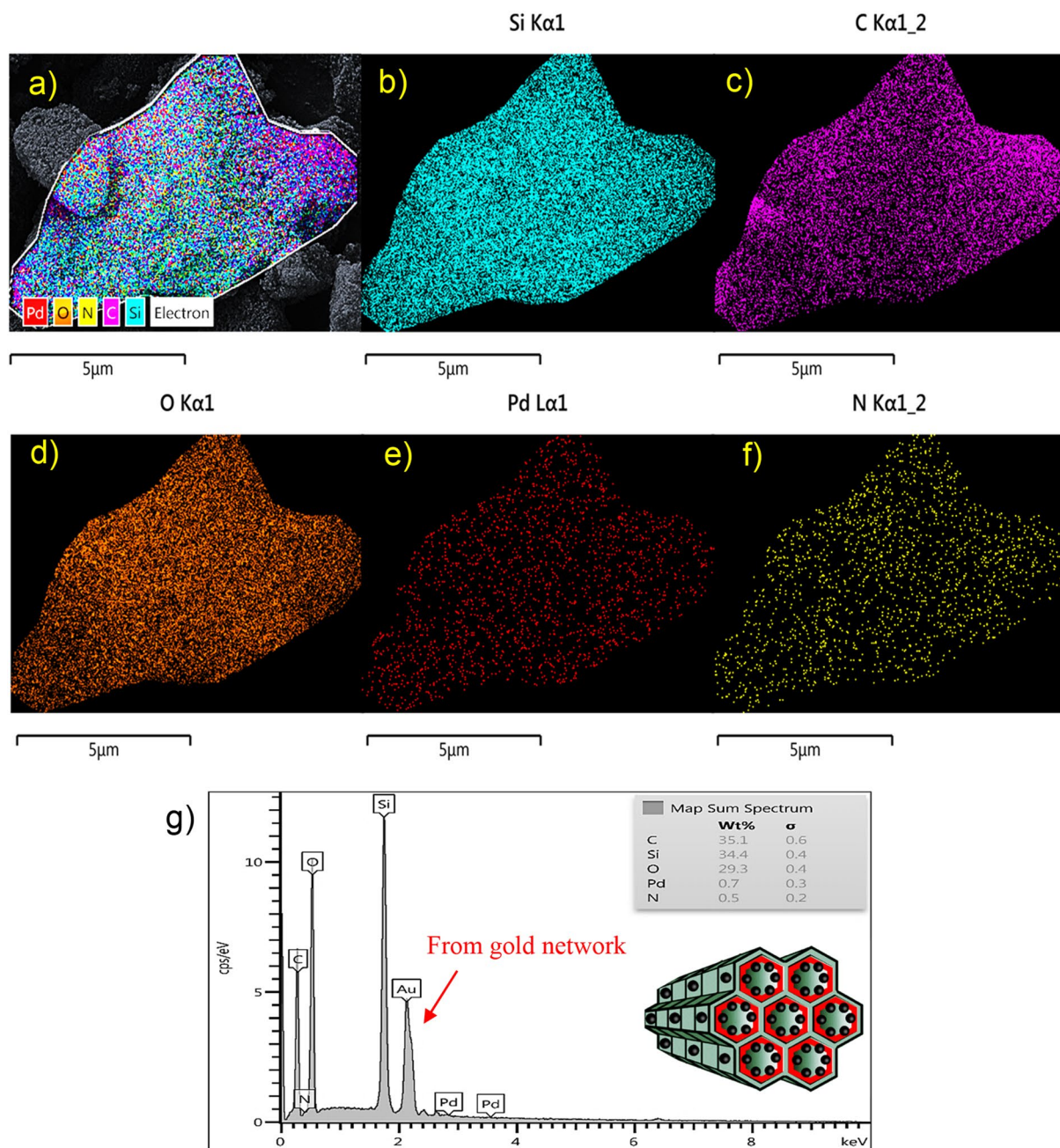


Figure 6. STEM/EDS-mapping micrograph (a–f) and EDX analysis of Pd@Kryf/MCM-41 (g).

To expand the scope of reaction substrates, a series of aryl halide derivatives were coupled with triphenyltin chloride in the presence of Pd@Kryf/MCM-41 catalyst (Table 2). The excellent conversion was obtained for all the desired biaryls without over homocoupling. Also, aryl halides with electron-donating and electron-withdrawing groups are well coupled with triphenyltin chloride, which indicates the reaction is not sensitive to the electronic effects. Besides, aryl iodides were found to be most reactive in comparison with aryl bromides and aryl chlorides, which such results were anticipated due to the high bond energy of the lighter halides^{60,61}. Furthermore, the sterically hindered aryl halides (entries 3, 5, and 10 Table 2) were good tolerated under the optimal reaction conditions. These results demonstrated that this reaction was not sensitive to both steric hindrance and electron effects, which shows a promising potential for practical application.

In order to examine chemoselectivity, the reaction of 3-bromobenzaldehyde with triphenyltin chloride was investigated in optimize conditions (Fig. 8a). The analysis of the mixture reaction after 12 h demonstrates that

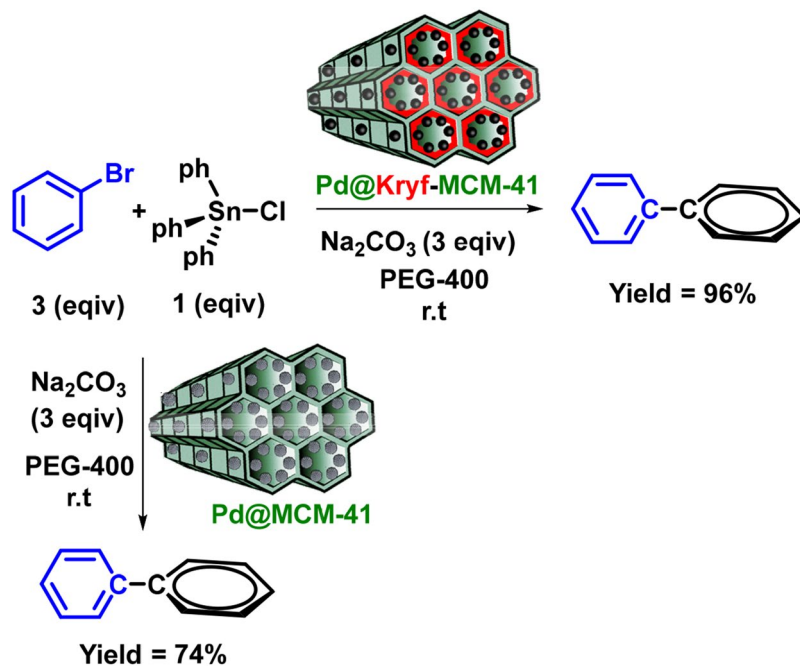
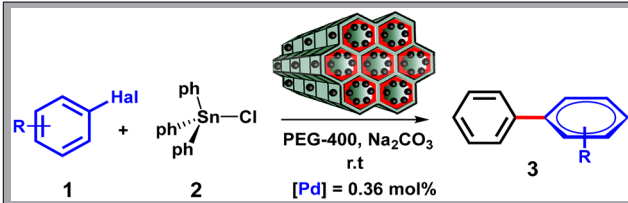


Figure 7. Synthesis of biaryls catalyzed by Pd@MCM-41 and Pd@Kryf/MCM-41.

Entry	Cat	Solvent	Base	T(°C)	Time (h)	TOF(h ⁻¹)/TON ^{tot}	Yield (%) ^b
1	none	PEG-400	Na ₂ CO ₃	25	24	–	N.R
2	Pd@Kryf/MCM-41	PEG-400	Na ₂ CO ₃ ^c	25	3	165/495	66
3	Pd@Kryf/MCM-41	PEG-400	Na₂CO₃	25	3	240/720	96
4	Pd@Kryf/MCM-41	PEG-400	Et ₃ N	25	3	180/540	72
5	Pd@Kryf/MCM-41	PEG-400	NaHCO ₃	25	3	178/534	71
6	Pd@Kryf/MCM-41	PEG-400	CaCO ₃	25	3	172/516	69
7	Pd@Kryf/MCM-41	PEG-400	NaOH	25	3	190/570	76
8	Pd@Kryf/MCM-41	Toluene	Na ₂ CO ₃	25	3	102/306	41
9	Pd@Kryf/MCM-41	<i>n</i> -hexane	Na ₂ CO ₃	25	3	90/270	34
10	Pd@Kryf/MCM-41	dioxane	Na ₂ CO ₃	25	3	65/195	26
11	Pd@Kryf/MCM-41	DMSO	Na ₂ CO ₃	25	3	83/249	33
12	Pd@Kryf/MCM-41	DMF	Na ₂ CO ₃	25	3	137/411	55
13	Pd@Kryf/MCM-41	EtOH	Na ₂ CO ₃	25	3	165/495	66
14	Pd@Kryf/MCM-41	H ₂ O	Na ₂ CO ₃	25	3	178/534	71
15	Pd ²⁺ @MCM-41	PEG-400	Na ₂ CO ₃	25	12	46/552	74
16	Pd ²⁺ @Kryf/MCM-41	PEG-400	Na ₂ CO ₃	25	12	48/576	77
17	Pd@Kryf/MCM-41	PEG-400	Na ₂ CO ₃	120	3	248/744	99

Table 1. Catalyst screening and reaction optimization for Stille coupling reaction^a. ^aReaction conditions: bromobenzene (3 equiv), Ph₃SnCl (1 equiv), Na₂CO₃ (3 equiv), PEG-400 (2 mL) in 0.36 mol% of catalyst. ^bIsolated yield of biaryls. ^cIn presence of 1 equiv Na₂CO₃.

biaryl product **3b** in a yield of 93% and corresponding benzophenone derivative **3a** was not observed. Moreover, chemoselectivity was further confirmed when 1-bromo-4-iodobenzene was employed as the reaction substrate (Fig. 8b). The reactions occurred exclusively with aryl iodides, but not aryl bromide and gave corresponding products **4a** with excellent yields. Furthermore, to evaluate the scalability of this catalytic system, the reaction



Entry	Hal	Ar-H	Product	%Yield ^b	TOF(h ⁻¹) ^c /TON ^{tot}	Melting point (°C)	Refs. ^d
1	I	Ph-	Ph-Ph	99(97) ^e	247/742	71–72	28,40
2	I	<i>p</i> -Me-Ph-	<i>p</i> -Me-Ph-ph	98	245/735	45–47	28,40
3	I	<i>o</i> -Me-Ph-	<i>o</i> -Me-Ph-Ph	98	245/735	Oil	28,40
4	I	<i>p</i> -MeO-Ph	<i>p</i> -MeO-Ph-Ph	98	245/735	87–89	28,40
5	I	<i>o</i> -MeO-Ph	<i>o</i> -MeO-Ph-Ph	97	242/727	Oil	28,40
6	I	<i>p</i> -MeCO-Ph	<i>p</i> -MeCO-Ph-Ph	96	240/720	121–123	28,40
8	I	<i>m</i> -NO ₂ -Ph	<i>m</i> -NO ₂ -Ph-Ph	94	235/705	60–62	28,40
9	Br	Ph-	Ph-Ph	96(82)	240/720	71–73	28,40
10	Br	<i>o</i> -MeO-Ph	<i>o</i> -MeO-Ph-Ph	94	235/705	Oil	28,40
11	Br	<i>m</i> -CHO-Ph-	<i>m</i> -CHO-Ph-Ph	93	232/697	57–59	28,40
12	Br	<i>m</i> -NO ₂ -Ph	<i>m</i> -NO ₂ -Ph-Ph	90	225/675	60–62	28,40
13	Br	<i>p</i> -MeCO-Ph	<i>p</i> -MeCO-Ph-Ph	91	227/682	121–123	28,40
14	Br	1-Br-Naphtalene	1-Ph-Naphtalene	90	225/675	Oil	
15	Cl	Ph-	Ph-Ph	89(87) ^e	222/667	71–73	28,40
16	Cl	<i>p</i> -Me-Ph	<i>p</i> -Me-Ph-Ph	85	212/637	45–47	28,40

Table 2. Coupling of aryl halides with Ph₃SnCl catalyzed by Pd@Kryf/MCM-41^a. ^aReaction conditions: **1** (3 mmol), **2** (1 mmol), catalyst (0.36 mol% Pd), Na₂CO₃ (3 mmol), PEG-400 (2 ml), r.t. ^bIsolated yield of biaryls. ^cTOF reaction was calculated as mmol of product formed per mmol of the catalyst at unit time. ^dEarlier reference of the corresponding product. ^ePd@MCM-41 was applied.

was performed in 30 mmol scales, which conversion biphenyl in 91% (Fig. 8c). These findings indicate that the present protocol is a chemoselective, sustainable, and large-scale application.

The catalytic activity of Pd@Kryf/MCM-41 was also compared with best catalyst systems reported in the literature (Table 3). The proposed catalyst indicated an excellent catalytic activity than most of the reported works. It is evident that Pd particles in sub-nanometric scales reveal an excellent catalytic activity in terms of yield, reaction time, and catalyst load.

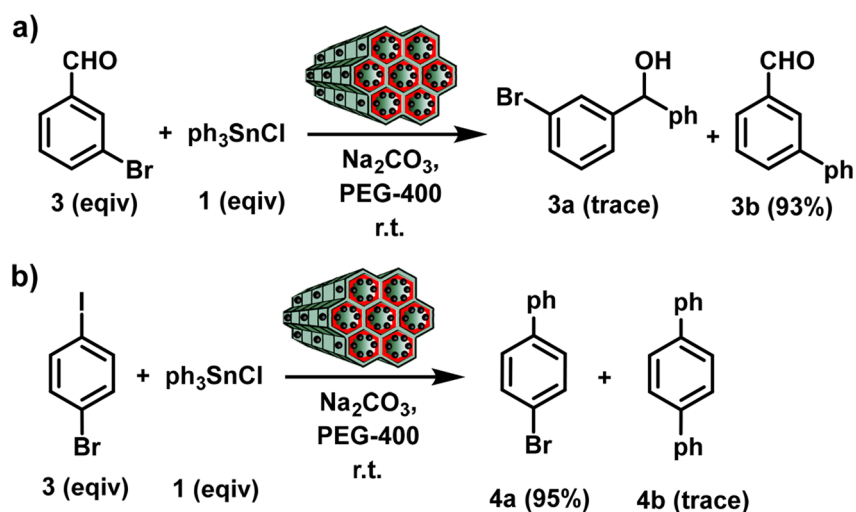
Proposed mechanism of Stille coupling reactions. To further develop the mechanism of action Pd NPs in coupling reactions, a plausible mechanism for Stille coupling using Pd@Kryf/MCM-41 was presented in Fig. 9a. The oxidative addition of aryl halides to Pd⁽⁰⁾Kryf/MCM-41 is the initial step to give complex Pd and intermediate II. After that, an organotin reagent reacts with intermediate II in transmetalation to afford intermediate III. Finally, reductive elimination of intermediate III gives biaryl product and Pd⁽⁰⁾Kryf/MCM-41. In the presence of Kryf ligand, PEG-400 as a solvent, and a base (Na₂CO₃), probably the stable anionic complexes [Pd⁰@kryf] are formed, which can accelerate the oxidative addition of aryl halides with Ph₃SnCl⁶⁰. Furthermore, X-ray photoelectron spectrum (XPS) analysis was used to identify the status of Pd in Pd@Kryf/MCM-41. After completing the Stille coupling reaction, the Pd 3d region exhibited two typical peaks centered at 336.98 and 342.38 eV, which can be ascribed to 3d_{5/2} and 3d_{3/2} states of Pd (0) respectively⁶⁹ (Fig. 9b).

Recyclability of the catalyst. The stability and reusability are key factors in practical application that must be considered for an effective catalytic system. To this end, the catalyst was separated by centrifuge after each use and prepared for the subsequent cycle. As shown in Fig. 10a, the activity was maintained for the first six times, suggesting that the catalyst was stable during coupling reaction. Furthermore, stable mesoporous silica material after the reuse was confirmed by FESEM (Fig. 10b) and TEM images (Fig. 10c–e). Besides, ICP-OES results indicate that after each cycle, the leaching of Pd is below 1.0 ppm (Table S2, ESI), which shows excellent physicochemical stability during Stille coupling reaction.

Conclusions

We indicated that Kryptofix 23 could be an excellent ligand for anchoring and stabilizing sub-nanometric Pd onto the pores of MCM-41. We also expanded an efficient protocol toward the economic synthesis of biaryls under sustainable conditions. This methodology revealed that the Pd@Kryf/MCM-41 has notable advantages such as excellent stability, negligible metal leaching, large scalability, and eco-friendly nature, which could coincide with

Chemoselectivity



High scalability

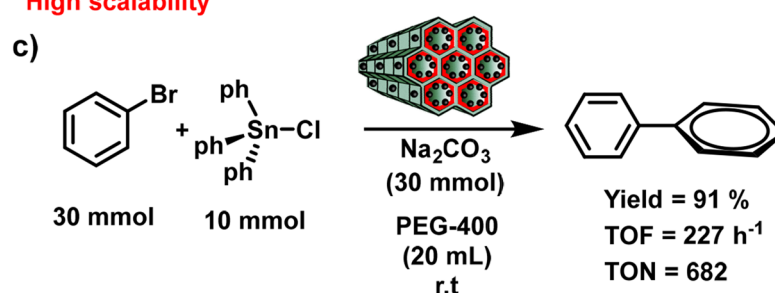


Figure 8. Chemoselectivity (a) and high scalability (b) of Pd@Kryf/MCM-41 in Stille coupling reaction.

Entry	Catalyst	Condition reaction	Yield (%)	Refs.
1	$\text{PdCl}_2(\text{PPh}_3)_2$	PEG, Na_2CO_3 , 90 °C	82	62
2	Pd NPs	PEG, K_2CO_3 , H_2O , 80 °C	90	63
3	$\text{Pd}(\text{OAc})_2$	Dabco, Bu_4NF , dioxane, 80 °C	93	64
4	Pd4 peptide	KOH, $\text{EtOH}/\text{H}_2\text{O}$, 25 °C	100	61
5	Pd@BTU-GO	NaOAc , PEG-400, 25 °C	94	17
6	HMS-CPTMS-Cy-Pd	PEG, K_2CO_3 , 100 °C	95	65
7	$\text{G}_3\text{DenP-Ni}$	CsF , H_2O , N_2 atm	98	66
8	$\text{Pd}/\text{Fe}_3\text{O}_4$	CsF , dioxane, 100 °C	86	67
9	$\text{Pd}_{\text{NR}}/\text{C}/\text{Fe}_3\text{O}_4$	DME, K_2CO_3 , 100 °C, 25 °C	95	68
10	Pd@Kryf/MCM-41	Na_2CO_3 , PEG-400, 25 °C	96	Present study
11	Pd@Kryf/MCM-41	Large-scale (30 mmol)	91	Present study

Table 3. Comparison of C–C coupling reaction with Pd@Kryf/MCM-41 and other reported systems.

the concepts of green chemistry. We envisage that the modifying of mesoporous silica pores with crown ether compounds for the stabilization of various colloidal metals can provide a new approach for the preparation of sustainable and environmentally friendly catalysts.

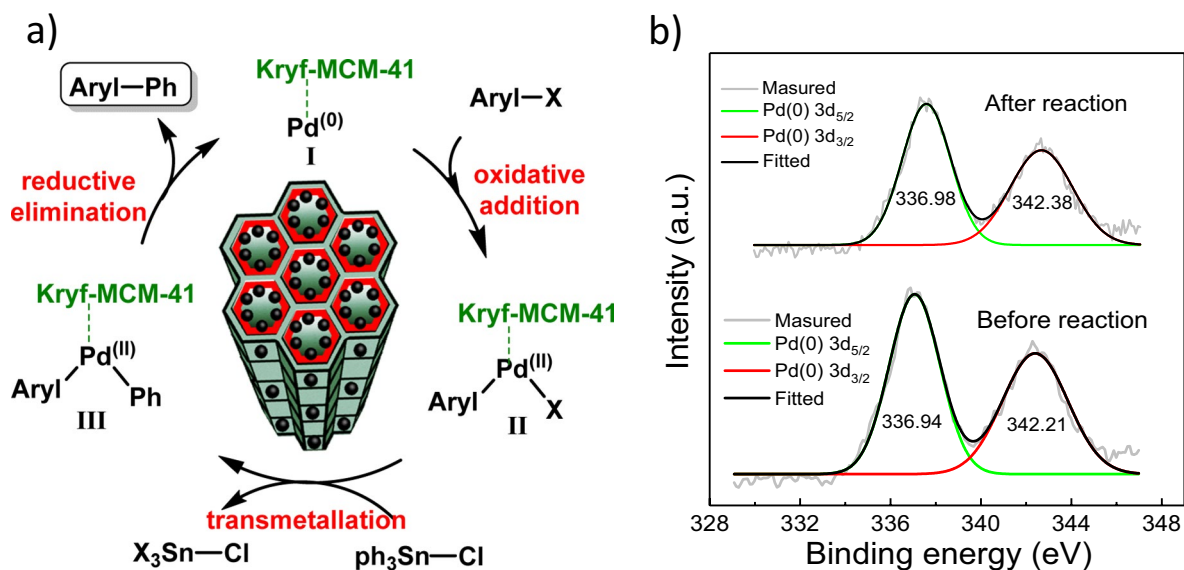


Figure 9. Proposed reaction mechanism for Stille reactions using Pd@Kryf/MCM-41 (a) and Pd 3d XPS of Pd@Kryf/MCM-41 before and after the reaction (b).

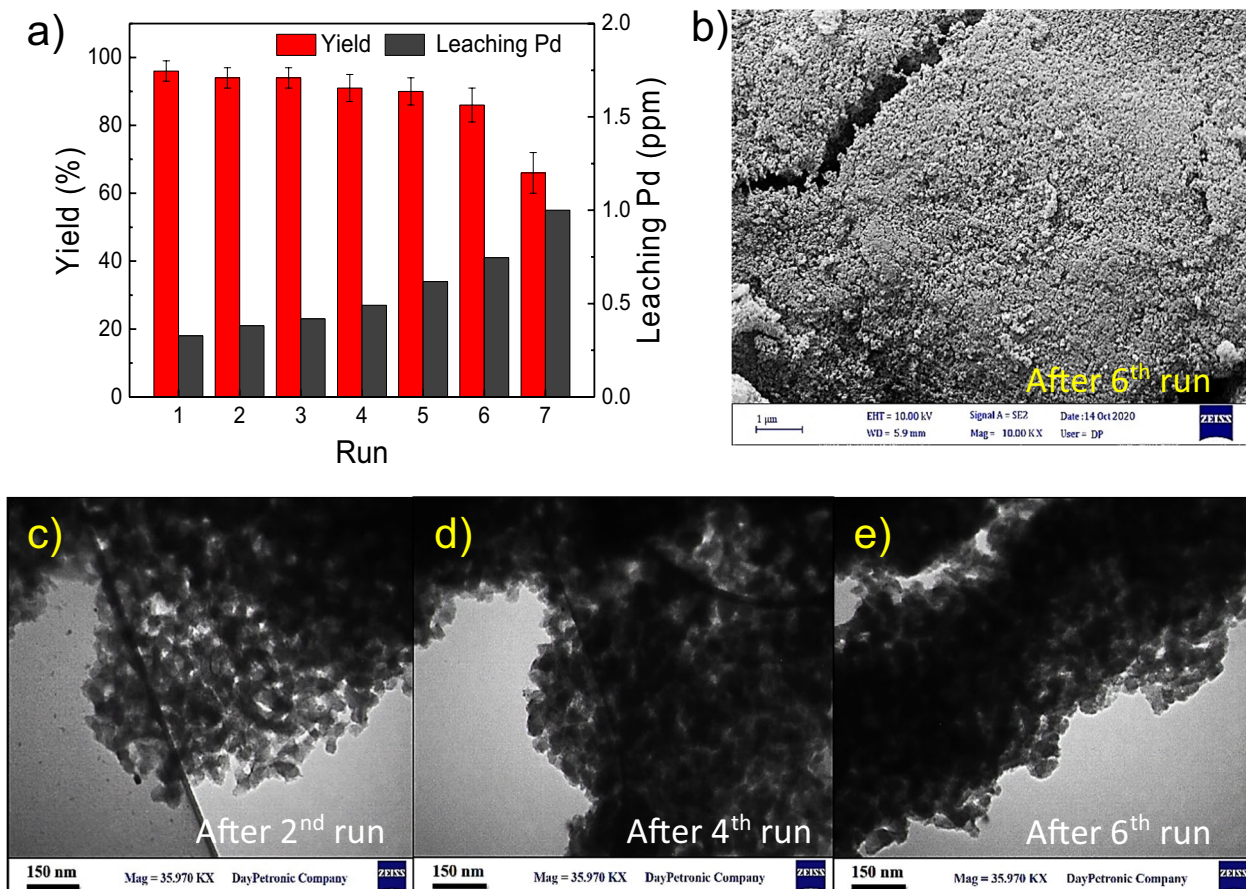


Figure 10. Recyclability of Pd@Kryf/MCM-41 for the synthesis of biaryls (a), FESEM (b), and TEM image of Pd@Kryf/MCM-41 (c–e).

Received: 5 May 2021; Accepted: 21 July 2021

Published online: 16 September 2021

References

- Corma, A. From microporous to mesoporous molecular sieve materials and their use in catalysis. *Chem. Rev.* **97**, 2373–2420 (1997).
- Ghimire, P. P. *et al.* Development of nickel-incorporated MCM-41–carbon composites and their application in nitrophenol reduction. *J. Mater. Chem. A* **7**, 9618–9628 (2019).
- Sun, L.-B., Liu, X.-Q. & Zhou, H.-C. Design and fabrication of mesoporous heterogeneous basic catalysts. *Chem. Soc. Rev.* **44**, 5092–5147 (2015).
- Chatterjee, M., Ishizaka, T. & Kawanami, H. Preparation and characterization of PdO nanoparticles on trivalent metal (B, Al and Ga) substituted MCM-41: Excellent catalytic activity in supercritical carbon dioxide. *J. Colloid Interface Sci.* **420**, 15–26 (2014).
- Rout, L., Mohan, A., Thomas, A. M. & Ha, C.-S. Rational design of thermoresponsive functionalized MCM-41 and their decoration with bimetallic Ag–Pd nanoparticles for catalytic application. *Microporous Mesoporous Mater.* **291**, 109711 (2020).
- Ghorbani-Choghamarani, A., Tahmasbi, B., Hudson, R. H. & Heidari, A. Supported organometallic palladium catalyst into mesoporous channels of magnetic MCM-41 nanoparticles for phosphine-free CC coupling reactions. *Microporous Mesoporous Mater.* **284**, 366–377 (2019).
- Rungsi, A. N. *et al.* Tuning the porosity of sulfur-resistant Pd–Pt/MCM-41 bimetallic catalysts for partial hydrogenation of soybean oil-derived biodiesel. *Fuel* **298**, 120658 (2021).
- Mori, K., Yamaguchi, T., Ikurumi, S. & Yamashita, H. Positive effects of the residual templates within the MCM-41 mesoporous silica channels in the metal-catalyzed reactions. *Chem. Commun.* **49**, 10468–10470 (2013).
- Lin, X.-J. *et al.* In situ encapsulation of Pd inside the MCM-41 channel. *Chem. Commun.* **51**, 7482–7485 (2015).
- Wright, P. A., Morris, R. E. & Wheatley, P. S. Synthesis of microporous materials using macrocycles as structure directing agents. *Dalton Trans.* 5359–5368 (2007).
- Gnann, R. Z. *et al.* Naked fluoride ion sources: Synthesis, characterization, and coupling reaction of 1-methylhexamethylenetetramine fluoride. *J. Am. Chem. Soc.* **119**, 112–115 (1997).
- Clearfield, A., Sharma, C. K. & Zhang, B. Crystal engineered supramolecular metal phosphonates: Crown ethers and iminodiacetates. *Chem. Mater.* **13**, 3099–3112 (2001).
- Anzellotti, A., McFarland, A. & Olson, K. F. A rapid and simple colorimetric test for 2, 2, 2-cryptand (Kryptofix 2.2. 2.) in solution. *Anal. Methods* **5**, 4317–4320 (2013).
- Mozafari, R. & Ghadermazi, M. A nickel nanoparticle engineered CoFe₂O₄@GO–Kryptofix 22 composite: A green and retrievable catalytic system for the synthesis of 1, 4-benzodiazepines in water. *RSC Adv.* **10**, 15052–15064 (2020).
- Izatt, R. M., Pawlak, K., Bradshaw, J. S. & Bruening, R. L. Thermodynamic and kinetic data for macrocycle interactions with cations and anions. *Chem. Rev.* **91**, 1721–2085 (1991).
- Abalde-Cela, S., Carregal-Romero, S., Coelho, J. P. & Guerrero-Martínez, A. Recent progress on colloidal metal nanoparticles as signal enhancers in nanosensing. *Adv. Coll. Interface. Sci.* **233**, 255–270 (2016).
- Alamgholiloo, H., Rostamnia, S. & Pesyan, N. N. Anchoring and stabilization of colloidal PdNPs on exfoliated bis-thiourea modified graphene oxide layers with super catalytic activity in water and PEG. *Colloids Surfaces A Physicochem. Eng. Aspects* 125130 (2020).
- Jin, R., Zeng, C., Zhou, M. & Chen, Y. Atomically precise colloidal metal nanoclusters and nanoparticles: Fundamentals and opportunities. *Chem. Rev.* **116**, 10346–10413 (2016).
- Alamgholiloo, H. *et al.* Formation and stabilization of colloidal ultra-small palladium nanoparticles on diamine-modified Cr-MIL-101: Synergic boost to hydrogen production from formic acid. *J. Colloid Interface Sci.* **567**, 126–135 (2020).
- Vogler, A. Fluorescence of Kryptofix 5 metal complexes. *Inorg. Chem. Commun.* **51**, 78–79 (2015).
- Nakatsuji, Y. *et al.* Switching of cation selectivity toward Na⁺ and K⁺ by a new type of pH-responsive 16-crown-5 in a counter-current double uphill transport system. *J. Am. Chem. Soc.* **122**, 6307–6308 (2000).
- Mohamed, M. G. & Kuo, S.-W. Crown ether-functionalized polybenzoxazine for metal ion adsorption. *Macromolecules* **53**, 2420–2429 (2020).
- Aalinejad, M., Pesyan, N. N. & Doustkhah, E. Diaza crown-type macromolecule (kryptofix 22) functionalised carbon nanotube for efficient Ni²⁺ loading; A unique catalyst for cross-coupling reactions. *Mol. Catal.* **494**, 111117 (2020).
- Chakraborty, J., Nath, I. & Verpoort, F. Pd-nanoparticle decorated azobenzene based colloidal porous organic polymer for visible and natural sunlight induced Mott–Schottky junction mediated instantaneous Suzuki coupling. *Chem. Eng. J.* **358**, 580–588 (2019).
- Feng, Y. *et al.* Pd colloid grafted mesoporous silica and its extraordinarily high catalytic activity for Mizoroki–Heck reactions. *J. Mol. Catal. A: Chem.* **322**, 50–54 (2010).
- Alamgholiloo, H., Rostamnia, S. & Noroozi Pesyan, N. Extended architectures constructed of thiourea-modified SBA-15 nanoreactor: A versatile new support for the fabrication of palladium pre-catalyst. *Appl. Organomet. Chem.* **34**, e5452 (2020).
- Alamgholiloo, H. *et al.* Stepwise post-modification immobilization of palladium Schiff-base complex on to the OMS-Cu (BDC) metal–organic framework for Mizoroki–Heck cross-coupling reaction. *Appl. Organomet. Chem.* **32**, e4539 (2018).
- Rostamnia, S., Alamgholiloo, H. & Liu, X. Pd-grafted open metal site copper-benzene-1, 4-dicarboxylate metal organic frameworks (Cu-BDC MOF's) as promising interfacial catalysts for sustainable Suzuki coupling. *J. Colloid Interface Sci.* **469**, 310–317 (2016).
- Heravi, M. M. & Mohammadkhani, L. Recent applications of Stille reaction in total synthesis of natural products: An update. *J. Organomet. Chem.* **869**, 106–200 (2018).
- Ghorbani-Choghamarani, A., Aghavandi, H. & Mohammadi, M. Boehmite@SiO₂@Tris(hydroxymethyl)aminomethane-Cu (I): a novel, highly efficient and reusable nanocatalyst for the C–C bond formation and the synthesis of 5-substituted 1H-tetrazoles in green media. *Appl. Organomet. Chem.* **34**, e5804 (2020).
- Du, Z., Zhou, W., Bai, L., Wang, F. & Wang, J.-X. In situ generation of palladium nanoparticles: Reusable, ligand-free heck reaction in PEG-400 assisted by focused microwave irradiation. *Synlett* **2011**, 369–372 (2011).
- Mohammadi, M. & Ghorbani-Choghamarani, A. The first report of hercynite as a solid support, L-methionine-Pd complex supported on hercynite as highly efficient reusable nanocatalyst for C–C cross coupling reactions. *New J. Chem.* (2020).
- Edlová, T., Čubiňák, M. & Tobrman, T. Cross-coupling reactions of double or triple electrophilic templates for alkene synthesis. *Synthesis* **53**, 255–266 (2021).
- Lee, V. Application of copper (I) salt and fluoride promoted Stille coupling reactions in the synthesis of bioactive molecules. *Org. Biomol. Chem.* **17**, 9095–9123 (2019).
- Bhanja, P., Liu, X. & Modak, A. Pt and Pd nanoparticles immobilized on amine-functionalized hypercrosslinked porous polymer nanotubes as selective hydrogenation catalyst for α , β -unsaturated aldehydes. *ChemistrySelect* **2**, 7535–7543 (2017).
- Modak, A., Sun, J., Qiu, W. & Liu, X. Palladium nanoparticles tethered in amine-functionalized hypercrosslinked organic tubes as an efficient catalyst for suzuki coupling in water. *Catalysts* **6**, 161 (2016).
- Modak, A. & Bhaumik, A. Surface-exposed Pd nanoparticles supported over nanoporous carbon hollow tubes as an efficient heterogeneous catalyst for the CC bond formation and hydrogenation reactions. *J. Mol. Catal. A: Chem.* **425**, 147–156 (2016).
- Batmani, H., Pesyan, N. N. & Havasi, F. Ni-Biurea complex anchored onto MCM-41: As an efficient and recyclable nanocatalyst for the synthesis of 2, 3-dihydroquinazolin-4 (1H)-ones. *Microporous Mesoporous Mater.* **257**, 27–34 (2018).

39. Aghbash, K. O., Pesyan, N. N. & Batmani, H. Cu-kojic acid complex anchored to functionalized silica-MCM-41: A promising regioselective and reusable nanocatalyst for click reaction. *ACS Omega* **5**, 22099 (2020).
40. Bai, L. & Wang, J. X. Reusable, polymer-supported, palladium-catalyzed, atom-efficient coupling reaction of aryl halides with sodium tetraphenylborate in water by focused microwave irradiation. *Adv. Synth. Catal.* **350**, 315–320 (2008).
41. Alamgholiloo, H., Hashemzadeh, B., Pesyan, N. N., Sheikhmohammadi, A., Asgari, E., Yeganeh, J., & Hashemzadeh, H. A facile strategy for designing core-shell nanocomposite of ZIF-67/Fe₃O₄: A novel insight into ciprofloxacin removal from wastewater. *Process. Saf. Environ. Protect.* (2020).
42. Mohammadi, R. *et al.* Visible-light-driven photocatalytic activity of ZnO/g-C₃N₄ heterojunction for the green synthesis of biologically interest small molecules of thiazolidinones. *J. Photochem. Photobiol. A Chem.* **402**, 112786 (2020).
43. Alamgholiloo, H. *et al.* Boosting aerobic oxidation of alcohols via synergistic effect between TEMPO and a composite Fe₃O₄/Cu-BDC/GO nanocatalyst. *ACS Omega* **5**, 5182–5191 (2020).
44. Farajzadeh, M., Alamgholiloo, H., Nasibipour, F., Banaei, R. & Rostamnia, S. Anchoring Pd-nanoparticles on dithiocarbamate-functionalized SBA-15 for hydrogen generation from formic acid. *Sci. Rep.* **10**, 1–9 (2020).
45. Alamgholiloo, H., Pesyan, N. N., Mohammadi, R., Rostamnia, S. & Shokouhimehr, M. Synergistic advanced oxidation process for the fast degradation of ciprofloxacin antibiotics using a GO/CuMOF-magnetic ternary nanocomposite. *J. Environ. Chem. Eng.*, 105486 (2021).
46. Hashemzadeh, B., Alamgholiloo, Pesyan, N. N., Sheikhmohammadi, A., Asgari, E., Yeganeh, J., & Hashemzadeh, H. Degradation of ciprofloxacin using hematite/MOF nanocomposite as a heterogeneous fenton-like catalyst: A comparison of composite and core-shell structures. *Chemosphere*, 130970 (2021).
47. Beck, J. S. *et al.* A new family of mesoporous molecular sieves prepared with liquid crystal templates. *J. Am. Chem. Soc.* **114**, 10834–10843 (1992).
48. Ghosh, A., Patra, C. R., Mukherjee, P., Sastry, M. & Kumar, R. Preparation and stabilization of gold nanoparticles formed by in situ reduction of aqueous chloroaurate ions within surface-modified mesoporous silica. *Microporous Mesoporous Mater.* **58**, 201–211 (2003).
49. Khalil, K. M. S. Cerium modified MCM-41 nanocomposite materials via a nonhydrothermal direct method at room temperature. *J. Colloid Interface Sci.* **315**, 562–568 (2007).
50. Dai, B., Wen, B., Zhu, M., Kang, L. & Yu, F. Nickel catalysts supported on amino-functionalized MCM-41 for syngas methanation. *RSC Adv.* **6**, 66957–66962 (2016).
51. Hajian, R. & Ehsanikhah, A. Manganese porphyrin immobilized on magnetic MCM-41 nanoparticles as an efficient and reusable catalyst for alkene oxidations with sodium periodate. *Chem. Phys. Lett.* **691**, 146–154 (2018).
52. Evano, G., Theunissen, C. & Pradal, A. Impact of copper-catalyzed cross-coupling reactions in natural product synthesis: The emergence of new retrosynthetic paradigms. *Nat. Prod. Rep.* **30**, 1467–1489 (2013).
53. Ruiz-Castillo, P. & Buchwald, S. L. Applications of palladium-catalyzed C-N cross-coupling reactions. *Chem. Rev.* **116**, 12564–12649 (2016).
54. Hou, Z., Theyssen, N. & Leitner, W. Palladium nanoparticles stabilised on PEG-modified silica as catalysts for the aerobic alcohol oxidation in supercritical carbon dioxide. *Green Chem.* **9**, 127–132 (2007).
55. Cole-Hamilton, D. J. Homogeneous catalysis—new approaches to catalyst separation, recovery, and recycling. *Science* **299**, 1702–1706 (2003).
56. Wang, W.-B., Lu, S.-M., Yang, P.-Y., Han, X.-W. & Zhou, Y.-G. Highly enantioselective iridium-catalyzed hydrogenation of heteroaromatic compounds, quinolines. *J. Am. Chem. Soc.* **125**, 10536–10537 (2003).
57. Kumar, R., Chaudhary, P., Nimesh, S. & Chandra, R. Polyethylene glycol as a non-ionic liquid solvent for Michael addition reaction of amines to conjugated alkenes. *Green Chem.* **8**, 356–358 (2006).
58. Nambodiri, V. V. & Varma, R. S. Microwave-accelerated Suzuki cross-coupling reaction in polyethylene glycol (PEG). *Green Chem.* **3**, 146–148 (2001).
59. Chandrasekhar, S., Narsihmulu, C., Sultana, S. S. & Reddy, N. R. Poly (ethylene glycol)(PEG) as a reusable solvent medium for organic synthesis. Application in the Heck reaction. *Org. Lett.* **4**, 4399–4401 (2002).
60. Espinet, P. & Echavarren, A. M. The mechanisms of the Stille reaction. *Angew. Chem. Int. Ed.* **43**, 4704–4734 (2004).
61. Pacardo, D. B., Sethi, M., Jones, S. E., Naik, R. R. & Knecht, M. R. Biomimetic synthesis of Pd nanocatalysts for the Stille coupling reaction. *ACS Nano* **3**, 1288–1296 (2009).
62. Naghipour, A., Ghorbani-Choghamarani, A., Babaee, H., Hashemi, M. & Notash, B. Crystal structure of a novel polymorph of trans-dichlorobis (triphenylphosphine) palladium (II) and its application as a novel, efficient and retrievable catalyst for the amination of aryl halides and stille cross-coupling reactions. *J. Organomet. Chem.* **841**, 31–38 (2017).
63. Zhou, W.-J., Wang, K.-H. & Wang, J.-X. Pd (PPh₃)₄-PEG 400 catalyzed protocol for the atom-efficient Stille cross-coupling reaction of organotin with aryl bromides. *J. Org. Chem.* **74**, 5599–5602 (2009).
64. Li, J.-H. *et al.* Efficient Stille cross-coupling reaction catalyzed by the Pd (OAc)₂/Dabco catalytic system. *J. Org. Chem.* **70**, 2832–2834 (2005).
65. Gholamian, F. & Hajjami, M. Synthesis of Pd immobilized on functionalized hexagonal mesoporous silica (HMS-CPTMS-Cy-Pd) for coupling Suzuki-Miyaura and Stille reactions. *Polyhedron* **170**, 649–658 (2019).
66. Wu, L., Zhang, X. & Tao, Z. A mild and recyclable nano-sized nickel catalyst for the Stille reaction in water. *Catal. Sci. Technol.* **2**, 707–710 (2012).
67. Prasad, A. S. & Satyanarayana, B. Magnetically recoverable Pd/Fe₃O₄-catalyzed stille cross-coupling reaction of organostannanes with aryl bromides. *Bull. Korean Chem. Soc.* **33**, 2789–2792 (2012).
68. Kumar, B. S., Anbarasan, R., Amali, A. J. & Pitchumani, K. Isolable C@ Fe₃O₄ nanospheres supported cubical Pd nanoparticles as reusable catalysts for Stille and Mizoroki-Heck coupling reactions. *Tetrahedron Lett.* **58**, 3276–3282 (2017).
69. Powell, C. J. Recommended Auger parameters for 42 elemental solids. *J. Electron Spectrosc. Relat. Phenom.* **185**, 1–3 (2012).

Author contributions

H.A. wrote the main manuscript text and prepared figures. N.N.P and S.R. authors reviewed the manuscript.

Competing interests

The authors declare no competing interests.

Additional information

Supplementary Information The online version contains supplementary material available at <https://doi.org/10.1038/s41598-021-97914-z>.

Correspondence and requests for materials should be addressed to N.N.P. or S.R.

Reprints and permissions information is available at www.nature.com/reprints.

Publisher's note Springer Nature remains neutral with regard to jurisdictional claims in published maps and institutional affiliations.



Open Access This article is licensed under a Creative Commons Attribution 4.0 International License, which permits use, sharing, adaptation, distribution and reproduction in any medium or format, as long as you give appropriate credit to the original author(s) and the source, provide a link to the Creative Commons licence, and indicate if changes were made. The images or other third party material in this article are included in the article's Creative Commons licence, unless indicated otherwise in a credit line to the material. If material is not included in the article's Creative Commons licence and your intended use is not permitted by statutory regulation or exceeds the permitted use, you will need to obtain permission directly from the copyright holder. To view a copy of this licence, visit <http://creativecommons.org/licenses/by/4.0/>.

© The Author(s) 2021